Laboratory Observation of a Plasma-Flow-State Transition from Diverging to Stretching a Magnetic Nozzle

Kazunori Takahashi* and Akira Ando
Department of Electrical Engineering, Tohoku University, Sendai 980-8579, Japan
(Received 20 February 2017; revised manuscript received 18 April 2017; published 2 June 2017)

An axial magnetic field induced by a plasma flow in a divergent magnetic nozzle is measured when injecting the plasma flow from a radio frequency (rf) plasma source located upstream of the nozzle. The source is operated with a pulsed rf power of 5 kW, and the high density plasma flow is sustained only for the initial ~100 μ sec of the discharge. The measurement shows a decrease in the axial magnetic field near the source exit, whereas an increase in the field is detected at the downstream side of the magnetic nozzle. These results demonstrate a spatial transition of the plasma-flow state from diverging to stretching the magnetic nozzle, where the importance of both the Alfvén and ion Mach numbers is shown.

DOI: 10.1103/PhysRevLett.118.225002

The mutual interaction between a plasma flow and a magnetic field is one of the crucial fundamental processes related to particle acceleration and structure formation in various plasmas scaled up to astrophysics and down to laboratories. Plasma-flow-induced stretch of magnetic field lines is ubiquitous in naturally occurring plasmas such as the plasma ejection from the Sun, the magnetosphere surrounding Earth, and the astrophysical jets [1–4]. The magnetic field component along the plasma flow obviously increases for the stretched cases. However, typical laboratory static plasmas have exhibited diamagnetic properties [5–9]; i.e., the magnetic field component decreases and the field lines are diverged by the plasma, respectively.

The properties of plasmas affecting the magnetic field variation have also been an important topic related to momentum gain or loss processes and the development of a thruster utilizing a magnetic nozzle. The plasma in the magnetic nozzle is spontaneously accelerated by various types of acceleration processes [10–13]. When the plasma momentum is increased because of the interaction with the expanding magnetic fields, a reaction force is exerted on the magnetic field [14]. The plasma acceleration process is attributed to the diamagnetism of the plasma flow as demonstrated by direct measurements of the reaction force in laboratory experiments [15,16]. In such a configuration, as the applied magnetic field strength decreases and the plasma flow is accelerated along the expanding magnetic field, the ratio of the flow energy to the magnetic energy is expected to increase along the axis. For this situation, a magnetohydrodynamic (MHD) scenario and model have proposed that the plasma flow stretches the magnetic field lines to infinity, which is consistent with Alfvén's frozen-in theorem [17], and the plasma is detached from the applied field lines [18–20]. However, the magnetic field stretched by the plasma flow has not been observed in laboratory experiments, and the plasma detachment processes from the magnetic field lines have been discussed only based on the measured ion density and velocity in the magnetic nozzle [21–25]. Although other detachment scenarios have also been proposed [26,27], this issue remains unresolved.

To investigate the pure interaction between the plasma flow and the magnetic field with zero external electric current, measurement of the plasma-flow-induced axial magnetic field is performed in a magnetically expanding radio frequency (rf) plasma, where the plasma source is located upstream of the magnetic nozzle. Here we report a laboratory observation of the transition of the plasma-flow state from diverging to stretching the magnetic nozzle, where the former and latter occur near the source exit and in the downstream region of the magnetic nozzle, respectively. Laboratory experiments reveal that the transition occurs at the Alfvén Mach number of 0.2 ± 0.05.

Figure 1(a) shows a schematic of the experimental setup, where the plasma source is immersed in a 1-m-diameter and 2-m-long vacuum chamber. The source consists of a 64-mm-inner-diameter pyrex glass tube, an insulator back plate ($z = -16$ cm), a double-turn rf loop antenna ($z = -11$ cm), and a solenoid, where the downstream edge of the solenoid structure is defined as $z = 0$. The back plate has a small center hole and argon gas is continuously introduced into the source tube through the hole at a flow rate of 70 sccm; then the chamber pressure is maintained at ~0.6 mTorr. A dc current I_B is provided to the solenoid; the calculated magnetic field lines and strength B_z on the axis for $I_B = 4.5$ A are shown in Figs. 1(a) and 1(b), respectively. A pulsed rf power is fed to the antenna from a 13.56 MHz rf generator via a vacuum feedthrough and an impedance tuning circuit, where the pulse width and the repetition frequency are chosen as 5 msec and 10 Hz, respectively. The maximum rf power is $P_{\mathrm{rf}} \sim 5$ kW and the rising time of the rf generator is a few tens of μ sec.

A radially facing planar Langmuir probe (LP) and a B-dot probe (BP) are mounted on an axially and radially movable motor stage to measure the plasma density n_p and

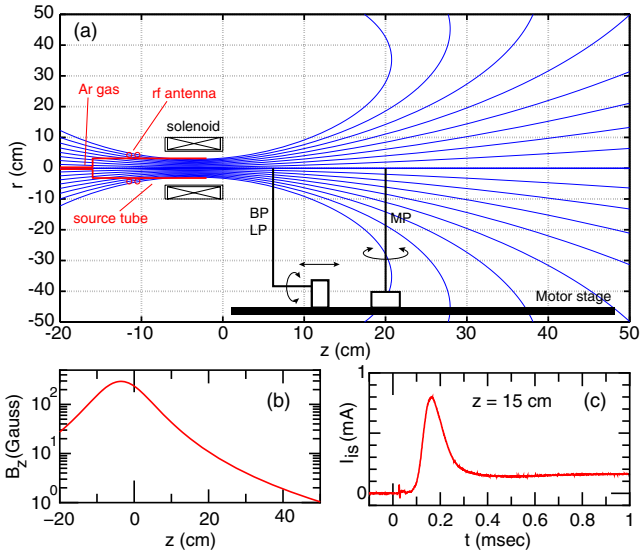

FIG. 1. (a) Schematic of the experimental setup together with the calculated magnetic field lines. (b) Axial profile of the magnetic field strength on axis for $I_B = 4.5$ A. (c) Typical temporal evolution of I_{is} of the LP located at $z = 15$ cm.

the plasma-induced axial magnetic field ΔB_z, respectively. Figure 1(c) shows the typical temporal evolution of the ion saturation current I_{is} of the LP at $z = 15$ cm, where the rf power is turned on at $t = 0$. As already reported, the ejection of the high density plasma from the source is sustained only for about a hundred of μsec because of a neutral depletion effect [28]. A low-pass filter with a cutoff frequency of ~50 kHz is used to remove high-frequency components from the BP signal and temporal integration of the signal gives the ΔB_z. Furthermore, a Mach probe (MP) consisting of two detection tips is mounted on another motor stage located at $z = 20$ cm as shown in Fig. 1(a), where the direction of the two tips is controlled by rotating the probe shaft. The ratio of the ion saturation currents of the two tips gives the ion Mach number, i.e., the plasma flow velocity normalized by the ion sound speed given by $C_s = \sqrt{k_B T_e/m}$. Here k_B, T_e, and m are the Boltzmann constant, the electron temperature, and the argon ion mass, respectively. The measured electron temperature of 5 eV gives $C_s \sim 3.5$ km/s.

Figure 2 depicts the measured spatiotemporal evolutions of (a) I_{is} and (b) ΔB_z for $I_B = 4.5$ A and $P_{rf} = 5$ kW,

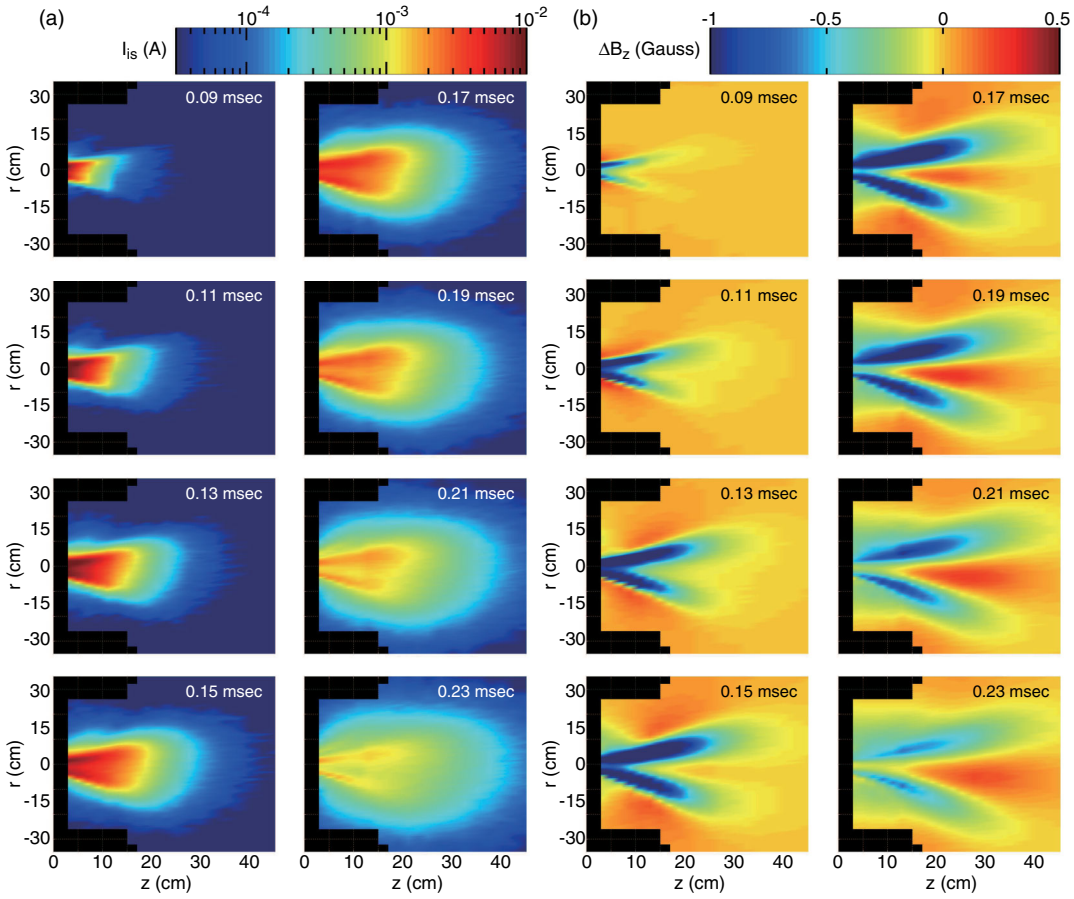

FIG. 2. Spatiotemporal evolution of (a) I_{is} and (b) ΔB_z, taken for $I_B = 4.5$ A and $P_{rf} = 5$ kW. The rf power is triggered at $t = 0$ and the signals are averaged over 16 shots, where the measurements are performed at ~1200 points (~20 points along z and ~60 points along r). A movie can also be found as Supplemental Material [29].

where the representative r-z profiles at every 0.02 msec are shown. The plasma expansion along the expanding magnetic field from the upstream to the downstream sides is clearly seen in Fig. 2(a). When the plasma exists only at the upstream region in the initial time of the discharge (typically $t \leq 0.15$ ms and $z < 15$ cm), the measured ΔB_z in Fig. 2(b) has a negative value at the radially central region, corresponding to the state diverging the magnetic nozzle. Once the plasma flow reaches the downstream side (typically $t \geq 0.17$ ms and $z > 15$ cm), an increase in the axial magnetic field (positive ΔB_z) is clearly observed in the radially central region. $z > 15$ cm corresponds to the state stretching the magnetic nozzle, while the upstream diverging feature is still maintained at $z < 15$ cm. To the best of the authors' knowledge, the results in Fig. 2 are the first laboratory observation of the spatial transition of the plasma-flow state from diverging to stretching the magnetic nozzle.

To identify the transition condition, axial measurements of ΔB_z and I_{is} are performed for various magnetic field strength and plasma densities, which are controlled by I_B and P_{rf}, respectively. It should be noted that the radial position of the BP and LP is adjusted so as to obtain measurements at the radial center of the ΔB_z profile, since the profile is slightly asymmetric as seen in Fig. 2(b), which is probably due to the radial asymmetry of the density profile [Fig. 2(a)] and the misalignment of the setup. Typical temporal evolutions of the axial profile of ΔB_z for the different I_B are indicated with contour color in Figs. 3(a) and 3(b), where the black solid lines show the contour lines of $\Delta B_z = 0$, i.e., the transition between the two states in the z-t plane. Although the axial position of the transition temporally moves as in Figs. 3(a) and 3(b) because of the temporally varying density [see Fig. 1(c)], the transition in Fig. 3(a) is clearly found to occur more upstream than that occurring in Fig. 3(b). The time corresponding to the temporal peak in I_{is} [seen in Fig. 1(c)] is also plotted as a function of z [open squares together with the fitted linear lines in Figs. 3(a) and 3(b)], which gives the propagation velocity of the density peak. The velocity estimated from the fitted lines for the tested conditions is 2 ± 0.15 km/s and is unchanged by the external parameters of I_B and P_{rf}; no clear change of the velocity along z is observed within the accuracy of the present measurements. Figure 3(c) depicts the measured ion Mach number as a function of the shaft angle ϕ of the MP, where the two tips face the upstream and downstream sides for $\phi = \pm 90°$, respectively, as illustrated in the upper inset. The detected ion Mach number of 0.55 and the ion sound speed of $C_s \sim 3.5$ km/s give a macroscopic axial flow velocity of 1.9 km/s, which fairly agrees with the propagation velocity obtained from Figs. 3(a) and 3(b). Figures 3(d) and 3(e) show the axial profiles of ΔB_z at the time of the maximum positive ΔB_z [white lines in Figs. 3(a) and 3(b)], as

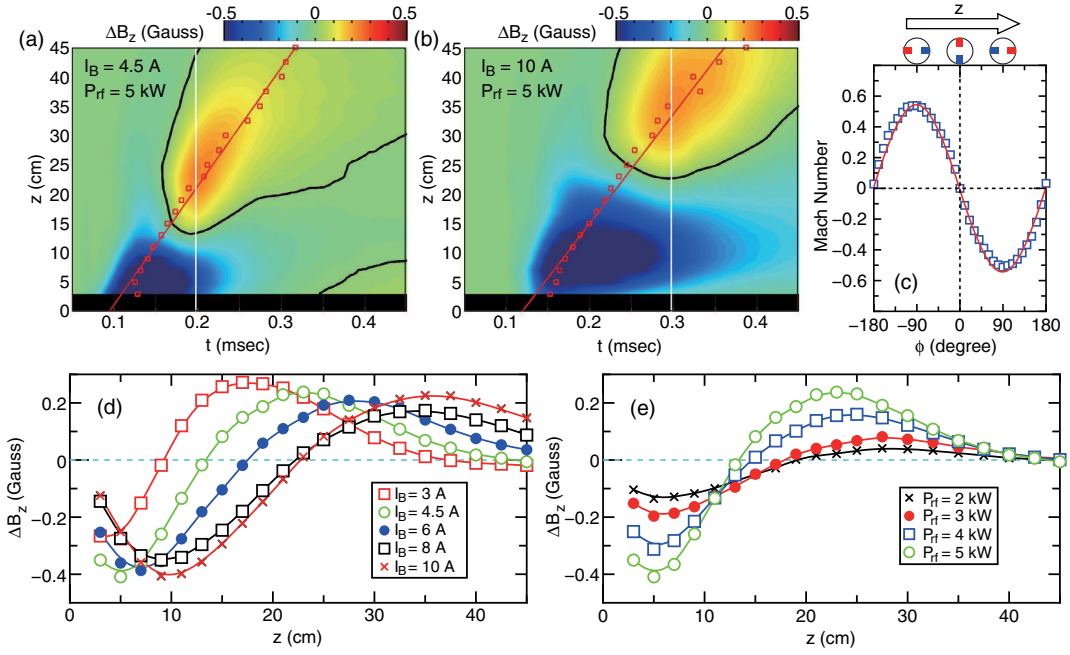

FIG. 3. (a),(b) Temporal evolutions of the axial profile of ΔB_z on axis for $I_B = 4.5$ and 10 A. Open squares are the times giving the temporal density peak as a function of z, and the fitted lines correspond to the propagation velocity of the density peak. White solid lines show the time giving the maximum ΔB_z. Black solid lines correspond to the contour lines of $\Delta B_z = 0$ implying the diverging-to-stretching transition. (c) Ion Mach number measured by the MP at $z = 20$ cm as a function of the rotational angle ϕ of the probe shaft together with the fitted sin function. (d),(e) Axial profiles of ΔB_z as functions of I_B and P_{rf}, where the data at the times giving the maximum ΔB_z [white solid lines in Figs. 3(a) and 3(b)] are plotted.

functions of I_B and $P_{\rm rf}$, respectively. These data indicate that the axial position of the transition depends on both the magnetic field strength and the plasma density.

The ratio β_k of the plasma flow energy $(mn_p v_z^2/2)$ to the magnetic energy $(B_z^2/2\mu_0)$ is a key parameter to discuss the magnetic field modification, where v_z and μ_0 are the axial plasma flow velocity and the permeability, respectively. It can also be rewritten as $\beta_k = (v_z/V_A)^2 = M_A^2$ with the Alfvén Mach number M_A, where V_A is the Alfvén velocity given by

$$V_A = v_z/M_A = B_z/\sqrt{\mu_0 m n_p}. \quad (1)$$

For the experimentally obtained plasma flow velocity of $v_z \sim 2$ km/s, Eq. (1) is drawn in the n_p-B_z^2 plane in Fig. 4 for various values of M_A. Furthermore, the measured plasma density n_p and the applied magnetic field strength B_z at the transition are plotted as filled squares in Fig. 4. The experimental data in Fig. 4 are close to $M_A \sim 0.2 \pm 0.05$, being less than unity. Since the transition in the expanding magnetic field is observed to occur for a constant Alfvén Mach number, the results show the MHD transition of the plasma-flow state from diverging to stretching the magnetic nozzle and identify the transition condition.

Here the transition to the stretching state for $M_A < 1$ is qualitatively discussed by the often used steady-state momentum equation in MHD approximation [30],

$$\rho(\mathbf{v}\cdot\nabla)\mathbf{v} = -\nabla p - \nabla B^2/2\mu_0 + (\mathbf{B}\cdot\nabla)\mathbf{B}/\mu_0, \quad (2)$$

where ρ and p are the mass density $(\sim m n_p)$ and the pressure $(\sim n_p k_B T_e)$, respectively. The last two terms on the right-hand side are the magnetic pressure and tension terms, respectively, which are derived from the $\mathbf{J}\times\mathbf{B}$ term and Ampere's law. When assuming a static plasma with no flow velocity and an almost uniform magnetic field, corresponding to the upstream side of the magnetic nozzle, Eq. (2) gives the well-known pressure equilibrium given by $\nabla(p + B^2/2\mu_0) = 0$. This shows the presence of the azimuthal diamagnetic plasma current and explains the negative ΔB_z near the source exit well. For the downstream limit of the magnetic nozzle, which allows the negligible magnetic and plasma pressure terms, the dimension analysis is carried out to discuss qualitatively. Equation (2) is then expressed as $|\rho v^2/L| \simeq |-B^2/\mu_0 L|$, with the scale length L of the gradient of all the physical parameters. This relationship can also be written as $v^2 \simeq V_A^2$ [31], which implies an increase in the magnetic field strength when the flow velocity exceeds the Alfvén velocity calculated with the applied magnetic field. This physical picture is also consistent with Alfvén's frozen-in theorem.

When all the terms in Eq. (2) are non-negligible, the dimension analysis gives $|\rho v^2/L| \simeq |p/L + B^2/2\mu_0 L - B^2/\mu_0 L| = |n_p k_B T_e/L - B^2/2\mu_0 L|$. Since this relationship can be written as $|v^2| \simeq |C_s^2 - V_A^2/2|$ and $V_A^2/2 > C_s^2$ is always satisfied in the present experiment, the equilibrium condition of

$$v^2 \simeq V_A^2/2 - C_s^2 \quad (3)$$

can be obtained, where C_s is constant for isothermal electrons. This indicates that the magnetic field lines are stretched when the square of the flow velocity exceeds $V_A^2/2 - C_s^2$. Equation (3) is now drawn by a bold dashed line in Fig. 4. The transition obtained from Eq. (3) occurs between $M_A = 0.3$ and 0.4; hence, the presently observed transition for $M_A < 1$ can be qualitatively explained by the MHD model. It is further noted that Eq. (3) can be expressed using only the Alfvén Mach number M_A and the ion Mach number M_i. Therefore, both M_A and M_i are important parameters affecting the transition. The above-described discussion is the rough estimation, but can explain the results qualitatively. Further detailed analysis will be required to quantitatively explain the results.

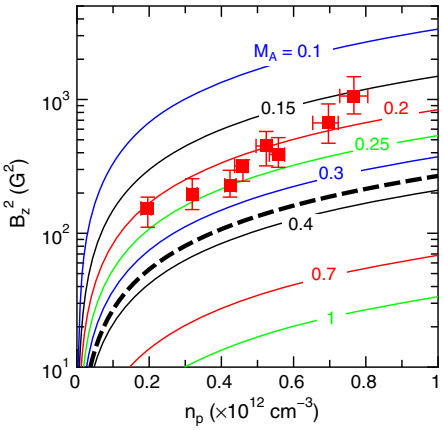

FIG. 4. Measured plasma density n_p and the square of the applied magnetic field strength B_z at the transition positions. The solid lines and the bold dashed line correspond to Eq. (1) for various values of the Alfvén Mach number M_A and Eq. (3), respectively, where the measured values of $v = 2$ km/s and $T_e = 5$ eV are used for the calculation.

In summary, the magnetic field induced by a plasma flow with a zero net discharge current is investigated in the magnetic nozzle. The results demonstrate the transition of the plasma-flow state from diverging to stretching the magnetic nozzle. Considering the momentum equation in the MHD approximation, both the Alfvén and ion Mach numbers affect the transition condition. This model is consistent with the experimental results presenting the diverging-to-stretching transition for the Alfvén Mach number of $M_A \sim 0.2 \pm 0.05$.

The authors would like to thank Professor C. Charles and Professor R. W. Boswell of Australian National University for their useful discussion. This work is partially supported

by grant-in-aid for scientific research (16H04084 and 26247096) from the Japan Society for the Promotion of Science, and the Yazaki Memorial Foundation for Science and Technology.

*kazunori@ecei.tohoku.ac.jp

[1] E. N. Parker, Astrophys. J. **128**, 664 (1958).
[2] Z. Mikic, D. C. Barnes, and D. D. Schnack, Astrophys. J. **328**, 830 (1988).
[3] A. Usadi, A. Kageyama, K. Watanabe, and T Sato, J. Geophys. Res. **98**, 7503 (1993).
[4] Y. Kato, S. Mineshige, and K. Shibata, Astrophys. J. **605**, 307 (2004).
[5] P. T. Lang K. Büchl, M. Kaufmann, R. S. Lang, V. Mertens, H. W. Müller, and J. Neuhauser (ASDEX Upgrade, NI Teams Collaboration), Phys. Rev. Lett. **79**, 1487 (1997).
[6] R. L. Stenzel and J. M. Urrutia, Phys. Plasmas **7**, 4450 (2000).
[7] C. S. Corr and R. W. Boswell, Phys. Plasmas **14**, 122503 (2007).
[8] B. R. Roberson, R. Winglee, and J Prager, Phys. Plasmas **18**, 053505 (2011).
[9] K. Takahashi, A. Chiba, A. Komuro, and A. Ando, Plasma Sources Sci. Technol. **25**, 055011 (2016).
[10] G. Hairapetian and R. L. Stenzel, Phys. Rev. Lett. **65**, 175 (1990).
[11] A. Sasoh, Phys. Plasmas **1**, 464 (1994).
[12] A. Fruchtman, Phys. Rev. Lett. **96**, 065002 (2006).
[13] C. Charles, R. W. Boswell, and R. Hawkins, Phys. Rev. Lett. **103**, 095001 (2009).
[14] E. Ahedo and M Merino, Phys. Plasmas **18**, 053504 (2011).
[15] K. Takahashi, T. Lafleur, C. Charles, P. Alexander, and R. W. Boswell, Phys. Rev. Lett. **107**, 235001 (2011).
[16] K. Takahashi, C. Charles, and R. W. Boswell, Phys. Rev. Lett. **110**, 195003 (2013).
[17] H. Alfvén, Ark. Mat. Astron. Fys. **29B**, 1 (1942).
[18] A. V. Arefiev and B. N. Breizman, Phys. Plasmas **11**, 2942 (2004).
[19] A. V. Arefiev and B. N. Breizman, Phys. Plasmas **12**, 043504 (2005).
[20] B. N. Breizman, M. R. Tushentsov, and A. V. Arefiev, Phys. Plasmas **15**, 057103 (2008).
[21] C. A. Deline, R. D. Bengtson, B. N. Breizman, M. R. Tushentsov, J. E. Jones, D. G. Chavers, C. C. Dobson, and B. M. Schuettpelz, Phys. Plasmas **16**, 033502 (2009).
[22] W. Cox, C. Charles, R. W. Boswell, and R. Haokins, Appl. Phys. Lett. **93**, 071505 (2008).
[23] K. Terasaka, S. Yoshimura, K. Ogiwara, M. Aramaki, and M. Y. Tanaka, Phys. Plasmas **17**, 072106 (2010).
[24] K. Takahashi, Y. Itoh, and T. Fujiwara, J. Phys. D **44**, 015204 (2011).
[25] C. S. Olsen, M. G. Ballenger, M. D. Carter, F. R. Chang Díaz, M. Giambusso, T. W. Glover, A. V. Ilin, J. P. Squire, B. W. Longmier, E. A. Bering III, and P. A. Cloutier, IEEE Trans. Plasma Sci. **43**, 252 (2015).
[26] E. B. Hooper, J. Propul. Power **9**, 757 (1993).
[27] M. Merino and E. Ahedo, Plasma Sources Sci. Technol. **23**, 032001 (2014).
[28] K. Takahashi, Y. Takao, and A. Ando, Appl. Phys. Lett. **108**, 074103 (2016).
[29] See Supplemental Material at http://link.aps.org/supplemental/10.1103/PhysRevLett.118.225002 for the movie of the spatiotemporal evolution of I_{is} and ΔB_z.
[30] A. M. Wright, Z. S. Qu, J. F. Caneses, and M. J. Hole, Plasma Phys. Controlled Fusion **59**, 025003 (2017).
[31] S. W. H. Cowley and D. J. Southwood, Geophys. Res. Lett. **7**, 833 (1980).